Research Article | Vol. 12, No. 6 / 1 June 2021 / Biomedical Optics Express 3241
Biomedical Optics EXPRESS

Toward a quantitative method for estimating tumour-stroma ratio in breast cancer using polarized light microscopy

JILLIAN SPRENGER,[1] CIARA MURRAY,[2] JIGAR LAD,[1] BLAKE JONES,[1] GEORGIA THOMAS,[1] SHARON NOFECH-MOZES,[3] MOHAMMADALI KHORASANI,[4,7] AND ALEX VITKIN[1,5,6,7,*]

[1]*Department of Medical Biophysics, University of Toronto, Toronto, Canada*
[2]*Laboratory Medicine Program, University Health Network, Ontario, Canada*
[3]*Department of Laboratory Medicine and Pathobiology, University of Toronto, Toronto, Canada*
[4]*Department of Surgery, University of British Columbia, Victoria, Canada*
[5]*Division of Biophysics and Bioimaging, Princess Margaret Cancer Centre, University Health Network, Toronto, Canada*
[6]*Department of Radiation Oncology, University of Toronto, Toronto, Canada*
[7]*Co-senior authors*
[*]*Alex.Vitkin@rmp.uhn.ca*

Abstract: The tumour-stroma ratio (TSR) has been explored as a useful source of prognostic information in various cancers, including colorectal, breast, and gastric. Despite research showing potential prognostic utility, its uptake into the clinic has been limited, in part due to challenges associated with subjectivity, reproducibility, and quantification. We have recently proposed a simple, robust, and quantifiable high-contrast method of imaging intra- and peri-tumoural stroma based on polarized light microscopy. Here we report on its use to quantify TSR in human breast cancer using unstained slides from 40 patient samples of invasive ductal carcinoma (IDC). Polarimetric results based on a stromal abundance metric correlated well with pathology designations, showing a statistically significant difference between high- and low-stroma samples as scored by two clinical pathologists. The described polarized light imaging methodology shows promise for use as a quantitative, automatic, and standardizable tool for quantifying TSR, potentially addressing some of the challenges associated with its current estimation.

1. Introduction

In recent years, extensive research efforts have been focused on identifying and developing new prognostic biomarkers for various types of cancer. Molecular-based prognostic and predictive tests have been used in subtypes of breast [1] and colon [2] cancer to identify patients at high risk of recurrence and select them for adjuvant chemotherapy; despite their high cost, some of these assays have been incorporated into clinical practice [3]. It has also become evident that the tumour microenvironment (TME) offers an additional rich source of prognostic information [4,5]. Solid tumours are comprised of more than just the tumour mass itself: the connective and supportive framework components also play a major role in tumour maintenance, growth, and metastasis [5,6]. Such stromal tissue components include the connective tissue matrix, collagen and elastin fibers, microvasculature, lymphatics and inflammatory cells, and fibroblasts among others.

One TME parameter that has been subject of multiple recent prognostication studies is the tumour-stroma ratio (TSR). This assessment of the quantity of stromal tissue relative to the quantity of tumour tissue (cellular-dense mass) has been shown to hold prognostic value in various solid organ cancers [7–17]. However, TSR is not routinely assessed in clinical practice

#422452 https://doi.org/10.1364/BOE.422452
Journal © 2021 Received 9 Feb 2021; revised 28 Apr 2021; accepted 1 May 2021; published 10 May 2021

Biomedical Optics EXPRESS

for solid tumours, although tumour cellularity is an important component of the Residual Cancer Burden Index that has gained clinical acceptance as a tool to examine breast carcinoma after presurgical systemic therapy [18]. In previous research studies, TSR is typically assessed in a semiquantitative manner by a pathologist viewing hematoxylin and eosin (H&E) stained slides. The pathologist selects specific regions of interest (ROIs) and then classifies these into two (or three) categories corresponding to high and low (or high, medium, and low) stroma based on pre-determined threshold values [8,16]. Although partly subjective and largely qualitative (categorical), TSR is a simple, inexpensive, and relatively quick metric to determine. The majority of TSR studies have found that patients with tumours containing higher amounts of stroma tend to have worse prognosis than those with lower amounts [10]. Its useful stromal information content may complement the more expensive and laborious prognostic (including molecular/genetic) tests that are currently in clinical use. Indeed, a robust and quantitative tool to quantify TSR can allow for further clinical studies and its potential incorporation as a marker that captures the prognostication information offered by the morphology of the tissue scaffolds surrounding the tumours.

However, despite its prognostic promise and research studies, the TSR's clinical uptake to date has been rather limited. This is due to the challenges of standardization in methodology, the reliance on pathologists' qualitative estimates, and the extra work burden the scoring process places on pathologists. This leads to difficulties with reproducibility, variability in results, and challenges in inter-study comparisons [13,19]. For example, variables such as H&E stain intensity, changes in microscopic examination conditions (e.g., 20x or 40x magnification) [13,19], and selection of ROIs within the tumour slide [13] are all known to influence results. Several groups have thus called for improved standardization and objectivity in TSR determinations [13,16,19]. Some methodologies mitigating these problems have been reported, for example by superimposing a grid with 300 random points on the selected ROI, and recording the tissue category (tumour, stroma, or other) at each point. The number of points in each tissue category was then tallied to determine the proportion of points in each [7,14,17]. However, this approach is time consuming and challenging to implement, and has not been widely adopted.

Our group has recently developed a novel method of polarized light microscopy to image and analyze the collagenous stroma in tumours [20–22], and has explored its utility in various TME-important biomedical contexts. For example, we have derived a *quantifiable stromal architecture signature score*, which was able to distinguish myxoid from sclerotic stroma, a differentiation of potential clinical significance [21]. Further, we have identified differences in *leading edge stromal alignment* within ER-positive / HER2-negative (luminal) invasive breast cancer samples with low- and higher-risk of metastasis (as determined by OncotypeDX testing) [22]. Other groups have also recently used Mueller-matrix-based polarimetric methods to examine prostate [23], myocardial [24] and parenchymal [25] tissues and pathologies, often relying on advanced statistical, fractal and correlation analysis of measured depolarization patterns to discern relevant information. Our novel and simpler non-Mueller-matrix-based technique adds to this growing area of scientific interest and scholarship.

In this study, we apply our group's polarimetric method to examine *stromal abundance* in 40 unstained histology slides of human IDC, and test its correlation with the TSR scores determined by practicing pathologists from adjacent H&E-stained slides. Our approach attempts to address the primary issues associated with the current determination of TSR, namely its qualitative scoring method and subjectivity. If successful, this reproducible and quantitative methodology to separate between low-, medium-, and high-stroma groups warrants further study and validation. Eventually, it may enable a simple and robust tool for incorporating a stromal prognostic indicator into clinical use.

Biomedical Optics EXPRESS

2. Methods

2.1. Ethics

Institutional ethics approval was obtained from participating hospital institutions (University Health Network and Sunnybrook Hospital, both in Toronto, Ontario, Canada). The need for patients' consent to examine the breast cancer histopathology samples was waived by the ethics board due to the retrospective nature of the study and anonymization of personal health information.

2.2. Samples

This study used 40 archival surgical resection samples of ER-positive / HER2-negative IDC prior to any chemo- or radiation-therapy. The analysis used unstained 4.5 μm thick sections on charged slides, from formalin-fixed and paraffin-embedded (FFPE) blocks. Sample preparation involved chemical dewaxing to avoid possible polarization imaging artefacts [26]. No further processing was required for polarimetric imaging. Adjacent slides were H&E-stained and imaged at 20x magnification on an Aperio ScanScope CS (Leica Biosystems, USA) for the pathologists' ROI selection and TSR scoring.

2.3. ROI selection and TSR scoring

ROIs were chosen by a breast pathologist (CM), in a manner similar to prior TSR studies [8–12]. The pathologist viewed the H&E-stained adjacent slides and selected a rectangular ROI in the invasive front region of the tumour, ensuring that tumour cells were present on all four sides of the field of view consistent with previous TSR determination studies [19]. All ROIs across the 40 patient slides were similarly sized (~ 1mm x 0.5mm). Since the purpose of this study was not to assess the utility of the TSR as a prognostic factor, but rather to explore the ability of our polarimetric approach to quantitatively determine TSR, only one ROI per patient slide was chosen. The pathologist then estimated the proportion of stroma within the ROIs in increments of 10%, categorizing the slides in low (<40% stroma), medium (40-60%) and high (>60%) stroma groups. A second breast pathologist (SN-M) then independently re-scored the same ROIs. The pathologists were blinded to the polarimetry results, and the other study team members were blinded to the pathologists' scores.

The ROIs on the H&E images were used to locate the same ROI on the adjacent slide imaged polarimetrically. The ROIs were matched by eye using tissue "landmarks" (specific defining features of the region). Image processing and polarimetric analysis was then performed using MATLAB software (Mathworks, USA). Stromal abundance as quantified by polarimetry was hypothesized to correlate with the low-medium-high stroma categories determined by pathology.

2.4. Polarimetric method

Polarized light microscopy can enhance the contrast of birefringent materials (such as collagen) in a largely non-birefringent background of other tumoural structures. No staining or contrast agent is required. Imaging for this study was done using our group's novel polarimetric methodology previously described [20–22]. The process involves an AxioZoom V16 microscope (Zeiss, Germany), which is fitted with two linear polarizers (Thorlabs, LPVISE100-A) on computer-controlled motorized rotation mounts (PRM1.MZ8, Thorlabs, USA). The pathology slides are positioned between the two linear polarizers oriented perpendicular (crossed) relative to each other. The crossed polarizer pair is then rotated though 90°, stopping in 5° increments, and at each angular stop a polarimetric image is taken. Analysis of the resultant 18-image stack enables several parametric tissue images to be derived that are *independent of the measurement geometry*; that is, we remove the artefactual image contrast variations that depend on the crossed polarizers' orientation relative to the tissue's birefringent collagenous structures. The three parametric

Biomedical Optics EXPRESS

images thus derived reflect (1) birefringence (collagen) signal intensity, (2) its 2D orientation in the transverse plane, and (3) its abundance [20–22]. In this TSR study, the images of the third derived parameter, that of stromal abundance, were used.

2.5. Polarimetric image analysis and quantitative metrics extraction

Figure 1 presents an example of a derived polarimetric abundance image. The value, and thus the brightness, of any pixel in this image is proportional to the amount of birefringent connective tissue (in this case, collagenous stroma). It is calculated on a pixel-by-pixel basis, with a score of unity signifying a pixel that contains only birefringent tissue. As previously described [22], birefringent tissue exhibits an intensity modulation that follows

$$Intensity \propto \sin^2(2\tau) \tag{1}$$

where τ is the angle between the tissue's optical axis and the polarization direction of the analyser. Consequently, whether a given pixel denotes a birefringent tissue can be determined via a goodness-of-fit (R^2) comparison between the observed angular intensity variation and the theoretical dependence of Eq. (1). As such, this information can be used to separate out the collagenous stroma from other tissues using a simple threshold (above a certain goodness-of-fit value ~ stroma; below it ~ non-stromal tumorous tissue). Our previously chosen threshold value of $R^2 > 0.75$ proved to be a suitable differentiator [21], although a more rigorous approach to its selection is certainly possible. For the current study, this threshold helped calculate the fraction of the ROI containing birefringent tissue, by dividing the number of pixels with $R^2 > 0.75$ by the total number of pixels in the ROI. The resultant ratio was compared to pathologist's TSR categories.

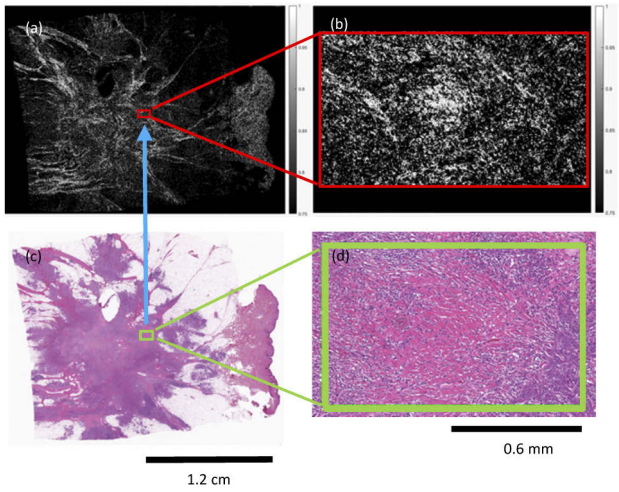

Fig. 1. Derived polarimetric abundance images and corresponding H&E images. (a) A full-slide polarimetric abundance image of human IDC derived from the stack of 18 angular crossed-polarizer unstained slide images. Brighter regions correspond to those with a higher amount of birefringent tissues (collagen). The red rectangle corresponds to the same ROI as that displayed by the green rectangle in (c), as indicated by the blue arrow. (b) The magnified polarimetric ROI. (c) An H&E-stained full-slide image corresponding to the image derived in (a). All H&E slides in this study were adjacent to those analyzed by polarimetry. (d) The magnified H&E ROI.

Biomedical Optics EXPRESS

2.6. Statistical methods

The pixel-wise abundance parameter was calculated for each ROI, typically yielding 60,000-90,000 values for each (number of pixels in each ROI). Then the ratio of pixels with an abundance score > 0.75 relative to the total pixel count was determined, and was recorded as the polarimetric estimate of TSR. These estimates were then compared across the pathologist-determined groups (high-, medium-, and low-stroma) using a non-parametric Kruskal-Wallis (KW) test (Mathworks, USA) [27,28]. This statistical method was used to test the null hypothesis that the data in categorical groups comes from the same distribution; it is intended for use with non-normally distributed data. A statistically significant result ($p < 0.05$) signifies that not all the samples come from the same distribution; in other words, that there are significant differences between at least some of the groups. A post-hoc pairwise comparison, performed with Tukey's test (Mathworks, USA) [27,29], identified which groups are different from each other. The entire statistical analysis was performed twice: each of the two pathologists' set of scores was treated independently, and was analyzed separately for correlation with polarimetry scores.

3. Results and discussion

The results of polarimetric imaging, analysis and quantification of stromal abundance in 40 unstained slides of IDC demonstrate the technique's ability to differentiate between stromal groups as scored by two clinical pathologists. Figure 2 shows the polarimetry-derived stromal abundance ratio for the three TSR groups, for each pathologist. For the first pathologist, the mean abundance score from the high-stroma group was highest at 0.44 ± 0.14 (mean ± standard deviation). The medium-stroma group yielded 0.41 ± 0.09, and the low-stroma group was 0.28 ± 0.13. The KW test indicated that not all groups come from the same distribution ($p = 0.012$). Post-hoc pairwise comparison indicated that a statistically significant difference was found between high- and low-stroma groups ($p = 0.014$); however, no significant difference was found between the polarimetric abundance scores of the medium-stroma group and the other two groups.

For the second pathologist, the polarimetric comparison yielded similar results. The mean abundance score from the high-stroma group was highest at 0.41 ± 0.14. The medium-stroma group yielded 0.39 ± 0.08, and the low-stroma group was 0.25 ± 0.13. Once again, the KW test indicated that not all groups come from the same distribution ($p = 0.025$). Similar to above, post-hoc pairwise comparison indicated that a statistically significant difference was found between high- and low-stroma groups ($p = 0.022$), but not between the polarimetric abundance scores of the medium-stroma group and the other two groups.

Despite some differences between the two pathologists' scores (discussed below), these results imply that polarimetry allows for a separation of low- and high-stroma groups. From a clinical perspective, this is encouraging. Most TSR studies have indicated that patients with less stroma tend to have better prognosis than those with its greater abundance [8–11]. This includes improved overall [9,10,15], disease-free [9,10,11,15], and distant metastasis-free survival [10]. With further development, it may be possible to use this method to derive TSR reliably, with promise of its utilization as a clinical prognostication tool.

While these are encouraging results, questions do remain over the significance of the medium-stroma group and our current inability to separate it out. It is interesting to note that a slightly different and commonly used Kolmogorov-Smirnov (KS) test (Mathworks, USA) [22,30] *does* indicate a significant difference between medium- and low-stroma groups for both pathologists, as visually suggested in Fig. 2 (p-values 0.008 and 0.018 respectively). However, here we chose to employ and report on the more rigorous and appropriate KW non-parametric test. Statistical analysis considerations aside, a recent study using low-, medium-, and high-stroma categories in rectal cancer found that patients in the medium-stroma group did perform poorly on certain outcome metrics (in some cases, even worse than those in the high-stroma group) [16]. Further

Biomedical Optics EXPRESS

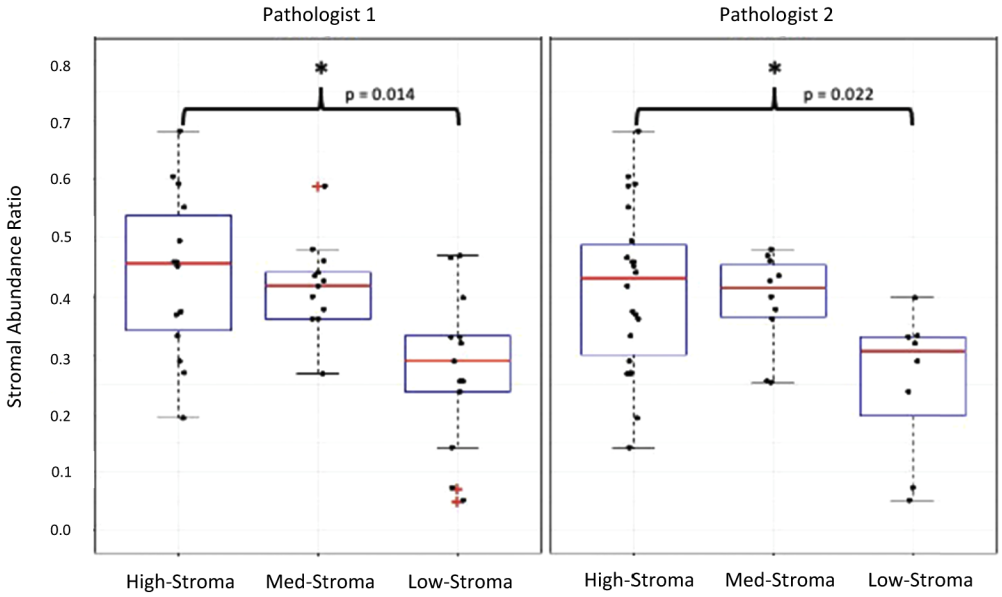

Fig. 2. Boxplots showing the comparisons of the polarimetrically-derived abundance metric to the three pathology-designated categories. For each group, the central red line shows the median, the blue box indicates the 1st and 3rd quartiles, the whiskers indicate the minimum and maximum values, and outliers are shown with a red "+". The * indicates a statistically significant difference ($p<0.05$). In the following data, μ represents the mean and σ represents standard deviation. (a) Boxplot for pathologist 1. For high-stroma: μ=0.44, σ=0.14, median=0.46; Medium-stroma: μ=0.41, σ=0.09, median=0.42; Low-stroma: μ=0.28, σ=0.13, median=0.29. There is a statistically significant difference between the high-stroma and low-stroma groups ($p = 0.014$). (b) Boxplot for pathologist 2. For high-stroma: μ=0.41, σ=0.14, median=0.43; Medium-stroma: μ=0.39, σ=0.08, median=0.41; Low-stroma: μ=0.25, σ=0.13, median=0.31. There is a statistically significant difference between the high-stroma and low-stroma groups ($p = 0.022$).

study is clearly needed to enable polarimetric separation of this potentially important group from the other two.

To better understand the detailed workings of this polarimetric stromal biomarker, we progress beyond the means analysis and explore the distributions of the pixel-wise abundance parameter for different pathologies. This is shown in Fig. 3, which displays stromal abundance results from representative (a) high-stroma and (b) low-stroma samples (as designated by both pathologists). As seen, the relative proportion of $R^2 > 0.75$ pixels (within the dotted rectangles) is indeed higher in (a) compared to (b), indicating a higher proportion of stromal pixels in accord with the pathology categories. But spatial heterogeneity is also evident from these distributions: in (a), and to a much greater extent in (b), a large fraction of pixels is clearly not described by the sinusoidal modulation of Eq. (1) characteristic of birefringent collagenous tissues. This is evidenced by the larger proportion of pixels in (b) with values outside the dotted red (stromal) rectangle. Our methodology's ability to detect and quantify these distributional differences in stromal content is indicative of its rich and potentially useful information content, over and above the currently used qualitative designations of overall average TSR categories (high, ±medium and low stroma).

Despite similar polarimetric performance in comparison with both pathologists, we now briefly examine the inter-pathologist variability of TSR scoring (Fig. 4(a)). As seen, overall the

Biomedical Optics EXPRESS

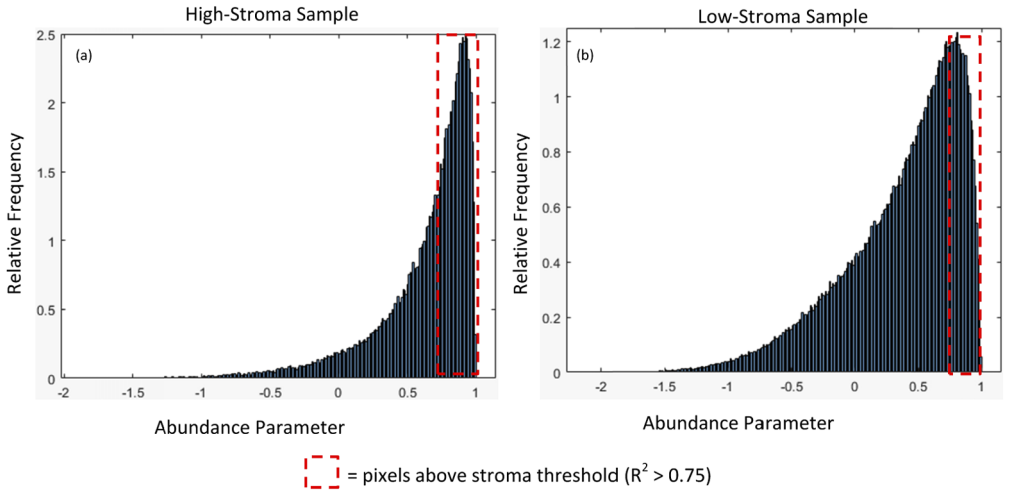

Fig. 3. Abundance parameter pixel value histograms from representative samples, presented as probability densities (area under curve = unity). Dotted red rectangles delineate the pixels above the 0.75 threshold that were considered 'stromal.' (a) An abundance histogram of a representative high-stroma sample. The rightward shift of values with a sharp peak indicates a large proportion of pixels conforming to the theoretical intensity modulation via Eq. (1), suggesting a region with high stromal content. The proportion of pixels contained in the dotted box is 0.49. (b) An abundance histogram for a representative low-stroma sample. The leftward shift of values indicates fewer pixels described by Eq. (1), as expected for a region with a low stromal content. The proportion of pixels contained in the dotted box is 0.24.

pathologists tend to agree in terms of classification of ROIs into high-, medium-, and low-stroma groups, but not in every case. This is further illustrated in Fig. 4(b), which shows pathologist agreement on more granular increments of 10%. The second pathologist's scores tend to be higher, and there are several outliers (e.g., one sample was scored as 10% by the first pathologist and 90% by the second). Figure 4(c) displays this ROI in question. Close visual examination reveals a conceptual disagreement: the paleomorphic tissue (consistent with extracellular mucin) is classified as "other" by one pathologist, and as stroma by the second.

Although not affecting our polarimetry-pathology correlation results, this inter-pathologist scores analysis illustrates the need for a robust and quantitative method of determining the TSR: despite an overall agreement between pathologists, there are ambiguities and challenges that must be addressed to allow stromal assessment usage in the clinic.

We now briefly consider possible reasons for our inability to unambiguously distinguish medium-stroma group from others. First, as discussed in the analysis of Fig. 2 above, a less-rigorous KS test *does* reveal its statistically-significant separation from the low-stroma group, so we are indeed 'close' to a robust low-medium-high three-group categorization. But perhaps the most plausible remaining obstacle is the variation in the "ground truth" (the pathologists' scores) as described above. Evidently, it is easier to identify a sample that has a clearly low or a clearly high TSR score. However, samples in the intermediate category are more difficult to classify qualitatively; that is, there may be sufficient subjectivity and variation in histology scoring so as to obscure any true differences between the medium-stroma and the other groups. It is also possible that morphological variations in similarly-scored regions are a factor, as illustrated in Fig. 5. The displayed ROIs were scored as 90% stroma by both pathologists; however, even to the untrained eye, there are obvious visual differences. These could lead to variations in the

Biomedical Optics EXPRESS

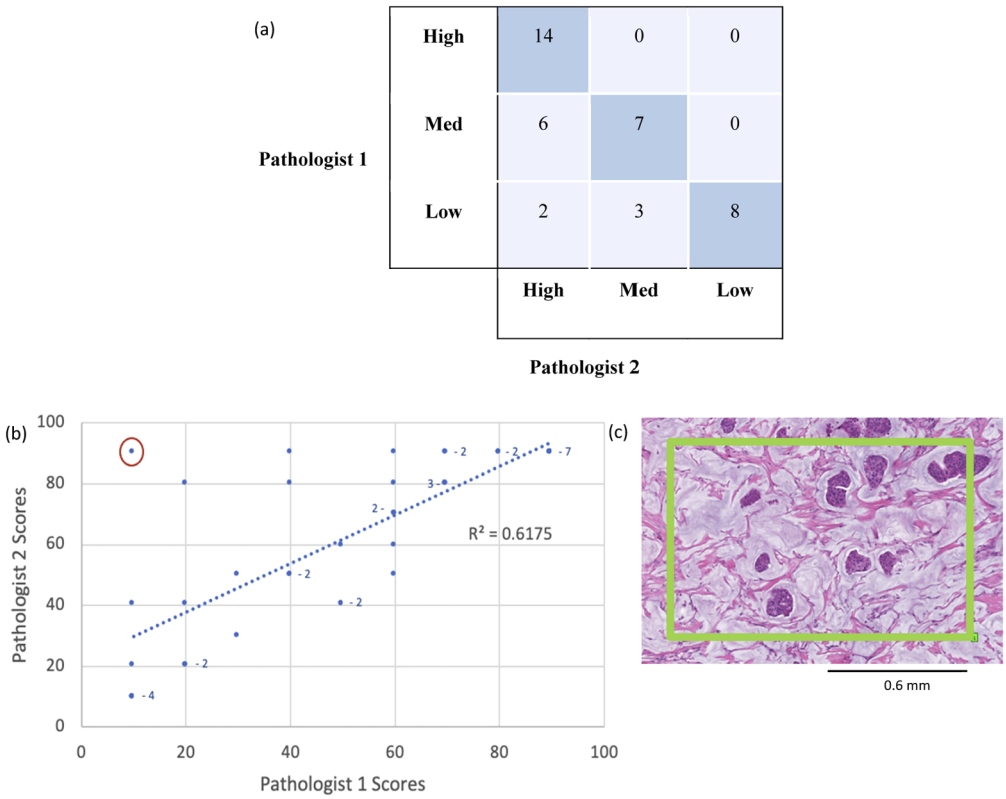

Fig. 4. (a) Agreement of pathologists on TSR classification of IDC samples. Each box shows the number of samples classified by the pathologist in that category. The pathologists agreed on the classification of 29 of the 40 samples (darker blue boxes). (b) Interpathology score comparisons, showing overall good agreement with notable exceptions (e.g., the circled ROI, whose TSR scores were 10% and 90%). The numbers beside some symbols indicate multiple data points with same scores. (c) ROI of one particular discrepant case (the one scored as 10% and 90% - see red circled point in (b)). The difference in classification stems from a lack of agreement over whether the paleomorphic tissue (consistent with extracellular mucin) should be classified as "stroma".

Biomedical Optics EXPRESS

corresponding polarimetric abundance scores, potentially contributing to the lack of difference between medium-stroma samples and the other groups.

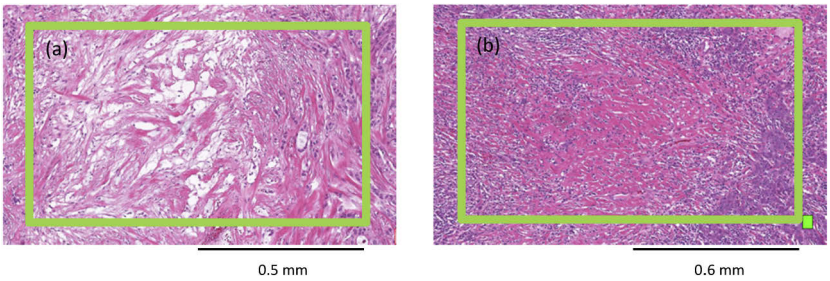

Fig. 5. Two ROIs scored as 90% stroma by both pathologists. (a) Despite its unanimous high-stroma designation, there are many "empty pockets" visible within this ROI. This is in contrast to (b), where the stromal fibers are more densely packed and no empty areas are seen. Such differences could affect both TSR and polarimetric scoring and contribute to our resultant inability to polarimetrically discriminate between high- and medium-stroma groups.

Despite our apparent inability to polarimetrically single out the medium-stroma group, the results are still encouraging. The polarimetric method allows for a separation of low- and high-stroma groups, which is interesting from a clinical perspective. As mentioned above, patients with less intratumoral stroma tend to fare better than those with more abundant stroma [8,10,11]. Reliably identifying "good" and "bad" prognostic groups may prove useful as a means of identifying low risk patients who do not require a molecular multi-gene assay, thus leading to a reduction in overall testing costs. With further development, this method may provide additional prognostic information for these patient cohorts.

Moving forward, we are exploring various means of gleaning additional information from our polarimetric images in order to improve quantitative separation between groups. One possibility being actively pursued in our lab is combining the abundance metric with others (e.g., alignment metric [20–22]) in order to enhance contrast between tissue types; the polarimetric alignment biomarker can highlight the presence and quantify the physical arrangement characteristics of stromal tissues in contrast to the cellular tumour compartment [20]. We are also exploring the utility of additional features of the pixel intensity distributions (Fig. 3), including higher orders of the central moment such as skewness and kurtosis [23–25]. Finally, we are investigating automatic (machine learning) methods for delineating tumour boundaries and selecting ROIs, in an effort to further "objectivize" our method by removing some subjectivity inherent in the pathologist-assisted ROI selection. These various methodological refinements will be necessary to test the ability of polarimetrically-determined TSR to predict clinical outcomes, and to address other clinically important questions.

There is currently a major push for automated digital techniques to replace or supplement pathologists' work in answering questions of clinical relevance. This is true in the context of TSR studies as well as in other pathology settings more broadly (e.g., detection and classification of various diseases [31,32] and tissue type classification based on computational image analysis [33], recently enhanced by increases in remote work during the Covid-19 pandemic [34]). In light of this, significant resources have been devoted to the development of new digital and computational methods. The polarimetric methods we are developing align well with this need for automation, computation, and standardization, providing an alternative to other emerging computational image analysis techniques being investigated [e.g., 33] as part of the larger digital pathology trend [31,32,34]. In this context, our approach is another potential route for assessing

Biomedical Optics EXPRESS

TSR, with its advantages of simplicity, ease of use, low cost, fast imaging/analysis times, high stromal contrast, quantification, and avoidance of potential staining artefacts.

4. Conclusion

The tumour-stroma ratio has been extensively studied and holds promise as a prognostic biomarker in various types of cancer. However, despite evidence suggesting its prognostic capabilities, there remain challenges that inhibit its widespread clinical uptake including its subjectivity and lack of standardization. We present a method of quantitatively assessing the stromal content in samples of invasive ductal carcinoma, using a novel polarimetric imaging technique. Our results show a statistically significant difference between high-and low-stroma groups (as scored by clinical pathologists) using just one polarimetry metric representing stromal abundance; the differential detection of medium-stroma cohort is close but currently not demonstrated. The ability to unequivocally separate various IDC patient cohorts is interesting scientifically and promising clinically, as for example there are different prognoses for patients with low versus high amounts of tumoural stroma. Future work will explore further morphological polarimetric quantification to improve the accuracy and the robustness of the resultant TSR scores, and investigate the possibility of automated ROI selection to minimize pathologists' subjectivity. Such refinements of the proposed polarized light imaging methodology could furnish a robust and reproducible stromal biomarker tool to assist pathologists in their prognostication and predictive studies of solid organ malignancies.

Funding. New Frontiers in Research Fund (NFRFE-2019-01049); Canadian Institutes of Health Research (PJT-156110); Natural Sciences and Engineering Research Council of Canada (RGPIN-2018-04930).

Acknowledgments. The authors would like to thank James Jonkman and the staff at the Advanced Optical Microscopy Facility of the University Health Network (Toronto, Canada). JS thanks the Canada Graduate Scholarships (CIHR) and the John H. Moss Scholarship for graduate studies support.

Disclosures. None.

Data availability. Data underlying the results presented in this paper are not publicly available at this time but may be obtained from the authors upon reasonable request.

References

1. K. S. Albain, W. E. Barlow, S. Shak, G. N. Hortobagyi, R. B. Livingston, I. Tien Yeh, P. Ravdin, R. Bugarini, F. L. Baehner, N. E. Davidson, G. W. Sledge, E. P. Winer, C. Hudis, J. N. Ingle, E. A. Perez, K. I. Pritchard, L. Shepherd, J. R. Gralow, C. Yoshizawa, C. Allred, C. K. Osborne, and D. F. Hayes, "Prognostic and predictive value of the 21-gene recurrence score assay in postmenopausal women with node-positive, oestrogen-receptor-positive breast cancer on chemotherapy: a retrospective analysis of a randomised trial," Lancet Oncol. **11**(1), 55–65 (2010).
2. J. M. O'Connell, I. Lavery, G. Yothers, S. Paik, K. M. Clark-Langone, M. Lopatin, D. Watson, F. L. Baehner, S. Shak, J. Baker, J. W. Cowens, and N. Wolmark, "Relationship between tumor gene expression and recurrence in four independent studies of stage II/III colon cancer patients treated with surgery alone or surgery plus adjuvant 5-FU/LV," J. Clin. Oncol. **28**(25), 3937–3944 (2010).
3. National Comprehensive Cancer Network. (2020). Breast cancer (version 4.2020). Retrieved from: https://www.nccn.org/professionals/physician_gls/pdf/breast.pdf
4. M. W. Conklin and P. J. Keely, "Why the stroma matters in breast cancer: insights into breast cancer patient outcomes through the examination of stromal biomarkers," Cell Adhes. Migr. **6**(3), 249–260 (2012).
5. D. Hanahan and L. M. Coussens, "Accessories to the crime: functions of cells recruited to the tumor microenvironment," Cancer Cell **21**(3), 309–322 (2012).
6. M. M. Mueller and N. E. Fusenig, "Friends or foes—bipolar effects of the tumour stroma in cancer," Nat. Rev. Cancer **4**(11), 839–849 (2004).
7. C. Downey, S. Simpkins, J. White, D. L. Holliday, J. L. Jones, L. B. Jordan, J. Kulka, S. Pollock, S. S. Rajan, H. H. Thygesen, A. M. Hanby, and V. Speirs, "The prognostic significance of tumour–stroma ratio in oestrogen receptor-positive breast cancer," Br. J. Cancer **110**(7), 1744–1747 (2014).
8. W. E. Mesker, J. M. Junggeburt, K. Szuhai, P. de Heer, H. Morreau, H. J. Tanke, and R. A. Tollenaar, "The carcinoma-stromal ratio of colon carcinoma is an independent factor for survival compared to lymph node status and tumor stage," Anal. Cell. Pathol. **29**(5), 387–398 (2007).
9. E. M. de Kruijf, J. G. H. van Nes, C. J. H. van de Velde, H. Putter, V. T. H. B. M. Smit, G. J. Liefers, P. J. K. Kuppen, R. A. E. M. Tollenaar, and W. E. Mesker, "Tumor–stroma ratio in the primary tumor is a prognostic factor in early

Biomedical Optics EXPRESS

breast cancer patients, especially in triple- negative carcinoma patients," Breast Cancer Res. Treat. **125**(3), 687–696 (2011).
10. C. Kramer, K. Vangangelt, G. W. van Pelt, T. Dekker, R. Tollenaar, and W. E. Mesker, "The prognostic value of tumour-stroma ratio in primary breast cancer with special attention to triple-negative tumours: a review," Breast Cancer Res. Treat. **173**(1), 55–64 (2019).
11. T. J. Dekker, C. J. van de Velde, G. W. van Pelt, J. R. Kroep, J. P. Julien, V. T. Smit, R. A. Tollenaar, and W. E. Mesker, "Prognostic significance of the tumor-stroma ratio: validation study in node-negative premenopausal breast cancer patients from the EORTC perioperative chemotherapy (POP) trial (10854)," Breast Cancer Res. Treat. **139**(2), 371–379 (2013).
12. K. Vangangelt, G. W. van Pelt, C. C. Engels, H. Putter, G. J. Liefers, V. Smit, R. Tollenaar, P. Kuppen, and W. E. Mesker, "Prognostic value of tumor-stroma ratio combined with the immune status of tumors in invasive breast carcinoma," Breast Cancer Res. Treat. **168**(3), 601–612 (2018).
13. M. Zengin, "Tumour budding and tumour stroma ratio are reliable predictors for death and recurrence in elderly stage I colon cancer patients," Pathol., Res. Pract. **215**(11), 152635 (2019).
14. C. L. Downey, H. H. Thygesen, N. Sharma, and A. M. Shaaban, "Prognostic significance of tumour stroma ratio in inflammatory breast cancer," SpringerPlus **4**(1), 68 (2015).
15. P. Aurello, G. Berardi, D. Giulitti, A. Palumbo, S. Maria Tierno, G. Nigri, F. D'Angelo, E. Pilozzi, and G. Ramacciato, "Tumor-Stroma Ratio is an independent predictor for overall survival and disease free survival in gastric cancer patients," The Surgeon **15**(6), 329–335 (2017).
16. R. Scheer, A. Baidoshvili, S. Zoidze, M. Elferink, A. Berkel, J. M. Klaase, and P. J. van Diest, "Tumor-stroma ratio as prognostic factor for survival in rectal adenocarcinoma: A retrospective cohort study," WJGO **9**(12), 466–474 (2017).
17. N. West, M. Dattani, P. McShane, G. Hutchins, J. Grabsch, W. Mueller, D. Treanor, P. Quirke, and H. Grabsch, "The proportion of tumour cells is an independent predictor for survival in colorectal cancer patients," Br. J. Cancer **102**(10), 1519–1523 (2010).
18. The University of Texas MD Anderson Cancer Center, "Residual cancer burden calculator," Clinical Calculators.
19. G. W. van Pelt, S. Kjær-Frifeldt, J. H. J. M. van Krieken, R. Al Dieri, H. Morreau, R. A. E. M. Tollenaar, F. B. Sørensen, and W. E. Mesker, "Scoring the tumor-stroma ratio in colon cancer: procedure and recommendations," Virchows Arch. **473**(4), 405–412 (2018).
20. J. Westreich, M. Khorasani, B. Jones, V. Demidov, S. Nofech-Mozes, and A. Vitkin, "Novel methodology to image stromal tissue and assess its morphological features with polarized light: towards a tumour microenvironment prognostic signature," Biomed. Opt. Express **10**(8), 3963–3973 (2019).
21. B. Jones, G. Thomas, J. Westreich, S. Nofech-Mozes, A. Vitkin, and M. Khorasani, "Novel quantitative signature of tumor stromal architecture: polarized light imaging differentiates between myxoid and sclerotic human breast cancer stroma," Biomed. Opt. Express **11**(6), 3246–3262 (2020).
22. B. Jones, G. Thomas, J. R. Sprenger, S. Nofech-Mozes, M. Khorasani, and I. A. Vitkin, "Peri-tumoural stroma collagen organization of invasive ductal carcinoma assessed by polarized light microscopy differs between OncotypeDX risk group," J. Biophotonics **13**(11), e202000188 (2020).
23. V. A. Ushenko, B. T. Hogan, A. Dubolazov, G. Piavchenko, S. L. Kuznetsov, A. G. Ushenko, Y. O. Ushenko, M. Gorsky, A. Bykov, and I. Meglinski, "3D Mueller matrix mapping of layered distributions of depolarization degree for analysis of prostate adenoma and carcinoma diffuse tissues," Sci. Rep. **11**(1), 5162 (2021).
24. V. A. Ushenko, B. T. Hogan, A. Dubolazov, A. V. Grechina, T. V. Boronikhina, M. Gorsky, A. G. Ushenko, Y. O. Ushenko, A. Bykov, and I. Meglinski, "Embossed topographic depolarization maps of biological tissues with different morphological structures," Sci. Rep. **11**(1), 3871 (2021).
25. M. Borovkova, L. Trifonyuk, V. Ushenko, O. Dubolazov, O. Vanchulyak, G. Bodnar, Y. Ushenko, O. Olar, O. Ushenko, M. Sakhnovskiy, A. Bykov, and I. Meglinski, "Mueller-matrix-based polarization imaging and quantitative assessment of optically anisotropic polycrystalline networks," PLoS One **14**(5), e0214494 (2019).
26. M. F. G. Wood, N. Vurgun, M. A. Wallenburg, and I. A. Vitkin, "Effects of formalin fixation on tissue optical polarization properties," Phys. Med. Biol. **56**(8), N115–N122 (2011).
27. M. Hollander and D.A. Wolfe, *Nonparametric Statistical Methods*, 3rd ed. (John Wiley & Sons, 2013).
28. Mathworks USA. (2021). Kruskal-Wallis Test. Retrieved from: https://www.mathworks.com/help/stats/kruskalwallis.html
29. Mathworks USA. (2021). Multiple Comparison Test. Retrieved from: https://www.mathworks.com/help/stats/multcompare.html
30. Mathworks USA. (2021). Two-Sample Kolmogorov-Smirnov Test. Retrieved from: https://www.mathworks.com/help/stats/kstest2.html
31. L. Pantanowitz, A. Sharma, A. B. Carter, T. Kurc, A. Sussman, and J. Saltz, "Twenty years of digital pathology: an overview of the road travelled, what is on the horizon, and the emergence of vendor-neutral archives," J. Pathol. Inform. **9**(1), 40 (2018).
32. L. Barisoni, K. J. Lafata, S. M. Hewitt, A. Madabhushi, and U. G. J. Balis, "Digital pathology and computational image analysis in nephropathology," Nat. Rev. Nephrol. **16**, 669–685 (2020).
33. S. Reis, P. Gazinska, J. H. Hipwell, T. Mertzanidou, K. Naidoo, N. Williams, S. Pinder, and D. J. Hawkes, "Automated classification of breast cancer stroma maturity from histological images," IEEE Trans. Biomed. Eng. **64**(10), 2344–2352 (2017).

Biomedical Optics EXPRESS

34. L. Browning, R. Colling, E. Rakha, N. Rajpoot, J. Rittshcer, J. A. James, M. Salto-Tellez, D. R. J. Snead, and C. Verrill, "Digital pathology and artificial intelligence will be key to supporting clinical and academic cellular pathology through COVID-19 and future crises: the PathLAKE consortium perspective," J. Clin. Pathol., Epub ahead of print, 2020.